Evaluating Track-Following Servo Performance of High-Density Hard Disk Drives Using Patterned Media

Younghee Han and Raymond A. de Callafon

Department of Mechanical and Aerospace Engineering, University of California at San Diego, La Jolla, CA 92093-0401 USA

In recent years, track densities of magnetic hard disks have continued to grow. A promising approach to continuing the trend to ultrahigh density is using bit-patterned media (BPM). However, the implementation of BPM in hard disk drives (HDDs) to achieve high recording density is challenging and requires various new techniques, such as new servo pattern designs and position error signal (PES) decoding schemes. In applying BPM in HDDs, it is important to select a servo pattern providing sufficient PES quality for head positioning. In this paper, we discuss evaluation of PES quality and servo pattern performance from a closed-loop (servo) point of view in order to evaluate the quality of several servo patterns. We consider three servo patterns (the amplitude pattern, chevron pattern, and differential frequency pattern) as case studies. We developed a PES simulation tool to provide a realistic HDD track-following simulation. Because of PES nonlinearity in the amplitude servo pattern, we considered time-based servo patterns as alternatives. For time-based servo patterns, we found that readback signal sampling and transition jitter greatly affect PES quality. Therefore, we conclude that the differential frequency servo pattern is superior to other patterns, since it is less sensitive to transition jitter and readback signal sampling.

***Index Terms*—Bit patterned media, hard disk drive, position error signal, servo patterns.**

I. Introduction

With THE continued growth of hard disk drive (HDD) track density, the thermal stability of magnetic recording media becomes an obstacle in achieving higher track densities. To achieve high thermal stability, patterned media has been proposed as a possible solution for ultra-high-density HDDs. Bit-patterned media (BPM) overcomes the thermal stability problem by creating predefined signal domain magnetic islands in which each bit is stored [1], [2]. In such high track density HDDs, a precise head track following performance is an important consideration. In the HDD head positioning system, the position error signal (PES) used in closed-loop control is obtained by demodulating readback signals generated from the servo patterns on disks. Thus, efficient servo pattern design and accurate estimation of PES are important for achieving good closed-loop servo track following performance. A number of studies on readback signal generation and PES evaluation have been conducted. Media noise sources and effects on readback signals were investigated in [3], [4]. PES nonlinearity due to nonlinear magnetoresistive (MR) heads was considered in [5]. Timing jitter caused by misalignment of servo burst patterns was mentioned in [6]. There is also a growing body of literature on BPM recording and performance evaluation of servo patterns for BPM recording. Basic recording physics, characteristics and advantages of a BPM recording are explained in [7]–[11]. Comparison of PES generation performance of different servo patterns for HDDs using BPM has been conducted in [12]–[14]. These researches show that patterned servo bits provide excellent PES recovery and allow us to use more advanced servo patterns. However, there has been little research on real integration of BPM in HDDs. It is important to select a servo pattern providing sufficient PES quality for head positioning when integrating BPM into HDDs.

The objective of this paper is to evaluate the quality of PES generated by several different servo patterns from a closed-loop (servo) point of view, thereby advancing the integration of BPM in HDDs by aiding in the selection of a servo pattern that provides sufficient PES quality. PES quality is evaluated by investigating important quality factors that have been thought to affect PES quality: amplitude fluctuation noise, transition jitter, signal sampling, and timing jitter. The procedure outlined in this paper is applicable to any servo pattern and any type of media. In this paper, the servo patterns are generated by modeling BPM. Results can be provided for discrete track media (DTM) or BPM, depending on the model used for the media. We select three different servo patterns (the amplitude pattern, chevron pattern, and differential frequency pattern [15]) as case studies to evaluate PES quality.

The paper is organized as follows. Approach to simulation is covered in Section II. In Section III, the evaluation of PES in a closed loop setting is explained. Section IV presents the results of PES simulation and discussions. Section V summarizes the conclusion of this paper.

II. Approach to Simulation

A. Readback Signal Generation

PES is obtained by demodulating a readback signal $R(t)$ generated from servo patterns embedded on HDDs. To compute a readback signal $R(t)$ from a servo pattern, two signals are used. In general, a readback signal $R(t)$ is calculated by the convolution of a transition response $h(t,w)$ and a bit pattern signal $b(t)$ determined by the actual servo patterns. Following [16], a readback signal $R(t)$ is modeled as a convolution

$$R(t) = \int h(t,w) \cdot \frac{d}{dt} b(t-\tau) d\tau$$

where $(d)/(dt)b(t-\tau)$ indicates the derivative of a bit pattern signal $b(t)$ due to the magnetic orientation. For longitu-

Manuscript received March 26, 2009; revised May 11, 2009. Current version published November 18, 2009. Corresponding author: Y. Han (e-mail: y3han@ucsd.edu).

Color versions of one or more of the figures in this paper are available online at http://ieeexplore.ieee.org.

Digital Object Identifier 10.1109/TMAG.2009.2025035

dinal recording, a transition response $h(t,w)$ is modeled as the Lorentzian pulse

$$h(t,w) = \frac{V_p}{1+\left(\frac{2t}{w}\right)^2}$$

where Vp is the peak value of the $h(t,w)$ and w is the width of $h(t,w)$ at half of its peak value. For perpendicular media, a transition response $h(t,w)$ can be modeled as [16]

$$h(t,w) = V_p \cdot \operatorname{erf}\left(\frac{2\sqrt{\ln 2}}{w}t\right)$$

where $\operatorname{erf}(x)$ is the error function, defined as

$$\operatorname{erf}(t) = \frac{2}{\sqrt{\pi}}\int_0^t e^{-x^2}dx.$$

To model the effect of different servo patterns and to be able to incorporate amplitude fluctuation noise, we propose to oversample a bit pattern signal $b(t)$. This provides a unique way to incorporate uncertainty into a readback signal $R(t)$. Using the notation $b(k)$ to indicate an oversampled bit pattern signal $b(k\Delta T)$ and a discrete-time convolution, we write a readback signal $R(k)$ via

$$R(k) = \sum_j h_{\Delta T}(j,w)\cdot[(b(k-j) - b(k-1-j)]$$

where $h_{\Delta T}(k,w)$ indicates the sampled transition response $h_{\Delta T}(k,w) = (1)/(\Delta T)\cdot h(k\Delta T, w)$.

Hence, once servo patterns are provided, a readback signal $R(k)$ can be generated from the servo patterns and can include uncertainty. With this approach we allow noise to occur on a bit pattern signal $b(k)$ to account for amplitude fluctuation noise and we can handle the transition jitter effect by modulating the time shift in a transition response $h(k,w)$. By including these effects we can study the sensitivity of each servo pattern.

B. Quality Measures for Readback Signals

In this paper, two sources of media noise are considered. The amplitude fluctuation noise and the transition jitter [3], [4]. Amplitude fluctuation noise is amplitude fluctuation on a bit pattern signal $b(k)$ due to magnetic nonuniformities of the media, as shown in Fig. 1(b). Various reasons, such as demagnetization field, media overwrite, adjacent track erasure (ATE), return-induced partial erase (RFPE), thermal fluctuation, etc., can affect amplitude fluctuation noise.

Using the notation $\aleph(\mu,\lambda)$ to indicate a normal distribution with a mean value μ and a variance λ, we model amplitude fluctuation noise $\eta(k)$ as independent and identically distributed (IID) samples from $\aleph(0,\lambda_\eta)$. Therefore, the bit pattern signal corrupted by amplitude fluctuation noise $\tilde{b}(k)$ is defined as $\tilde{b}(k) = b(k) + \eta(k)$, where $\eta(k) \sim \aleph(0,\lambda_\eta)$ and λ_η is the variance of amplitude fluctuation noise distribution. Therefore,

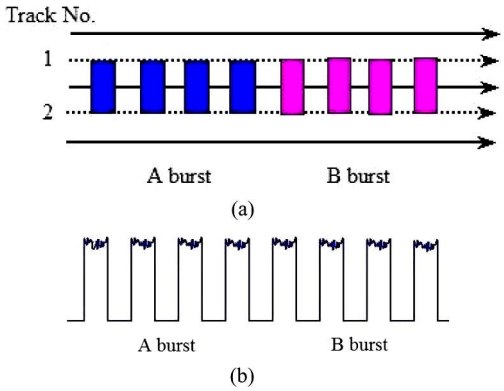

Fig. 1. (a) Servo pattern on a disk. (b) Bit pattern signal $b(k)$ with amplitude fluctuation noise generated from the servo pattern in (a).

the amplitude fluctuation noise effect on the readback signal $R(k)$ is modeled as

$$\begin{aligned}\tilde{b}(k) &= b(k) + \eta(k)\\ \eta(k) &\sim \aleph(0,\lambda_\eta)\\ R(k) &= \sum_j h_{\Delta T}(j,w)\cdot[\tilde{b}(k-j) - \tilde{b}(k-1-j)].\end{aligned} \quad (1)$$

Servo burst patterns contain the sequence of magnetic transitions. Random magnetization fluctuations in transition positions cause phase shift in a bit pattern signal $b(k)$. This random signal phase shift due to random transition position fluctuations is called transition jitter [3], [4], [16]. In this paper, we modulate time shifts in a transition response $h(k,w)$ to consider the transition jitter effect. Using the notation $\aleph(\mu,\lambda)$ as detailed above, we model transition jitter γ as IID samples from $\aleph(0,\lambda_\gamma)$ as $\tilde{h}_{\Delta T}(k,w) = h_{\Delta T}(\kappa,w), \kappa = k+\gamma$, where $\gamma \sim \aleph(0,\lambda_\gamma)$ and λ_γ is the variance of transition jitter distribution. Therefore, the transition jitter effect on a readback signal $R(k)$ is modeled as

$$\begin{aligned}\tilde{h}_{\Delta T}(k,w) &= h_{\Delta T}(\kappa,w), \kappa = k+\gamma\\ \gamma &\sim \aleph(0,\lambda_\gamma)\\ R(k) &= \sum_j \tilde{h}_{\Delta T}(j,w)[\tilde{b}(k-j) - \tilde{b}(k-1-j)].\end{aligned} \quad (2)$$

In the digital domain, readback signal sampling is another important quality factor in the evaluation of readback signal quality. The readback signal sampling interval ΔT is determined by how many samples are used to sample a bit pattern signal $b(k)$. Given total time T_p spent reading the bit pattern signal $b(k)$, the readback signal sampling interval ΔT is given by

$$\Delta T = \frac{T_p}{N_p} \quad (3)$$

where N_p is the number of samples. We will investigate the readback signal sampling effect on PES by changing the number of samples N_p. These quality factors (amplitude fluctuation noise, transition jitter and signal sampling) will be used to evaluate the quality of the readback signal $R(k)$ and PES from different servo patterns (the servo patterns performance).

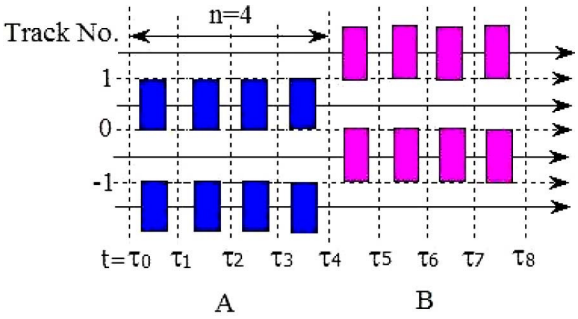

Fig. 2. Amplitude servo pattern.

Detailed simulation results of these effects will be presented in Section IV.

III. Closed-Loop PES Evaluation

A. Servo Patterns and Demodulation

An actuator controls the head position during track following. The head position is evaluated using servo patterns marked on the servo sectors. The PES sampling interval $\Delta\tau$ is determined by the location of servo sectors and the speed of the disk. For the analysis of PES quality, we assume the actuator stays on a single track due to track following mode. Since PES is obtained at the same servo sectors repeatedly as the disk rotates, the sampling time can be written as

$$t = (m + kN) \cdot \Delta\tau, m = 1, \ldots, N, k = 0, 1, \ldots$$

where m is a counter that indicates the mth servo sector at the specific track used for track following and N is the number of servo sectors. Using the notation e^m to indicate PES $e(t)$ for $t = (m + kN)\Delta\tau$, we write the time dependent PES $e(t)$ via

$$e^m = e(t), t = (m + kN) \cdot \Delta\tau.$$

If the servo sectors are equally spaced and the speed of the disk is constant, The PES sampling interval $\Delta\tau = (v/60)N$, where v is the speed of the disk. We will consider variation in the PES sampling interval $\Delta\tau$ to model the effect of timing jitter on PES e^m.

In this paper, the peak detection is employed to demodulate PES. The most commonly used servo pattern is the amplitude pattern which is shown in Fig. 2. The amplitude servo pattern contains two servo bursts: A and B. The shaded regions represent magnetized fields. When the read head passes these magnetic transitions, a readback signal $R(t)$ is generated.

Let the readback signals generated from A and B bursts at the mth servo sector be $R_A^m(t)$ and $R_B^m(t)$, respectively

$$R_A^m(t) = R^m(t) \quad \tau_0 < t < \tau_n$$
$$R_B^m(t) = R^m(t) \quad \tau_n < t < \tau_{2n}$$

and

$$\bar{R}_{Ai}^m = \max_{\tau_{i-1} < t < \tau_i} R_A^m(t), \quad i = 1, \ldots n$$
$$\bar{R}_{Bi}^m = \max_{\tau_{n+i-1} < t < \tau_{n+i}} R_B^m(t), \quad i = 1, \ldots n$$

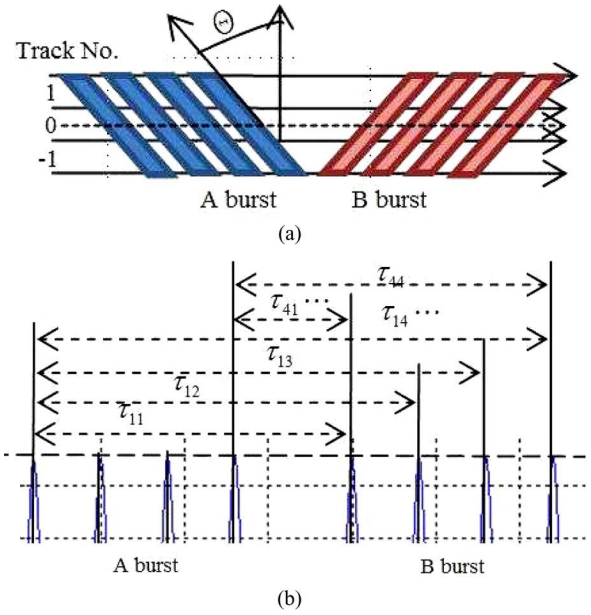

Fig. 3. (a) Chevron servo pattern. (b) Readback signal demodulation for the chevron servo pattern. τ_{ij} indicates the time from the ith pattern in A burst to the jth pattern in B burst.

where $R^m(t)$ is the readback signal generated from mth servo sector, n is the number of pulse in either A burst or B burst and m is the counter of servo sectors. The amplitudes of the readback signals generated from the A and B bursts vary with the position of the read head. The difference between the amplitudes of $R_A^m(t)$ and $R_B^m(t)$ is used to decode PES e^m as in [1] via

$$e^m = \sum_{i=0}^{n} \bar{R}_{Ai}^m - \bar{R}_{Bi}^m.$$

The amplitude servo pattern generates nonlinear responses to head positions due to MR heads' inherent nonlinearity [5]. Unlike the amplitude servo pattern, time based servo patterns show excellent linearity in responses to head positions across the entire track pitch. In this paper, chevron and differential frequency servo patterns will be considered. Many studies have been carried out on the chevron servo pattern [7], [8], [12]–[15]. As shown in Fig. 3, in the chevron pattern, parallel magnetic strips are symmetrically located across tracks generating two separate burst groups: A and B. The shaded regions represent magnetization.

Each pulse generated from a magnetic strip will be spatially aligned proportional to the amount of time between the strips. The relative time difference between these pulses is used to decode PES e^m as in [14] via

$$e^m = \sum_{p=1}^{n} \tau_{1p}^m + \sum_{p=1}^{n} \tau_{2p}^m + \cdots + \sum_{p=1}^{n} \tau_{np}^m - \bar{e}$$

where τ_{ij} indicates the time from the ith pattern in A burst to the jth pattern in B burst, as illustrated in Fig. 3(b). In addition $\bar{e}$ is the known time difference in case we were exactly at the middle of the pattern, indicated by dotted line in Fig. 3(a).

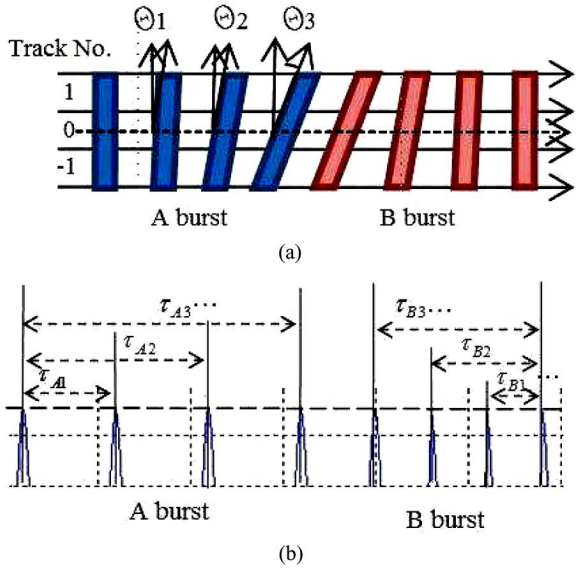

Fig. 4. (a) Differential frequency pattern. (b) Readback signal demodulation for the differential frequency pattern. τ_{Ai} indicates the time from the first bar in A burst to the rest of bars and τ_{Bi} indicates the time from the last bar in B burst to the rest of bars.

Another time-based servo pattern investigated in this paper is the differential frequency pattern and depicted in Fig. 4 [15]. This servo pattern also contains two separate burst groups: A and B. Each group includes four elongated magnetic strips. The shaded regions represent magnetized fields. The magnetized strips are positioned such that the first element of the A burst is placed orthogonal to the tracks and subsequent A burst elements are spaced apart such that they form an increasing angle relative to the tracks. The angle of the first element of the B burst is equal to the angle of the final element of the A burst and subsequent B burst elements form a decreasing angle relative to the tracks until the last element is positioned orthogonal to the tracks. As with the chevron servo pattern, each pulse generated from a magnetic strip will be spatially aligned proportional to the amount of time between the strips [15]. The relative time between these pulses is used to decode PES e^m via

$$T_A^m = \sum_{p=1}^{2(n-1)} \tau_{Ai}^m$$
$$T_B^m = \sum_{p=1}^{2(n-1)} \tau_{Bi}^m$$
$$e^m = T_A^m - T_B^m$$

where τ_{Ai} indicates the time from the first bar in A burst to the rest of bars and τ_{Bi} indicates the time from the last bar in B burst to the rest of bars.

B. Quality Measures for PES

In addition to the readback signal quality factors addressed in Section II-B, there are more quality factors to be considered in PES quality measurement. Depending on which servo patterns are used, MR heads' inherent nonlinearity causes nonlinearity in PES, thereby degrading PES quality. For more information on PES nonlinearity, one can refer to [5]. The PES quality is also affected by the timing-jitter caused by misalignment of the servo sector locations during HDD manufacturing. Due to manufacturing tolerances, servo sector locations can vary, therefore, the PES sampling interval $\Delta\tau$ is random instead of constant, resulting in degradation of PES quality due to timing jitter. In order to account for the timing jitter effect on PES quality, probability distributions of PES data positions (servo sector locations) are introduced. A dispersion parameter δ is used to model timing jitter by specifying the dispersion of the PES data (servo sectors) distributed on a disk. Using the dispersion parameter δ, asynchronous PES sampling becomes possible. The dispersion parameter δ is defined as

$$\sigma^2 = \left(\frac{2\pi\delta}{N}\right)^2 \tag{4}$$

where σ^2 is the variance of PES data position distribution and N is the number of servo sectors. Fig. 5 shows PES data position distributions at two successive servo sectors. If there is no dispersion in servo sector locations, the PES data positions will be exactly located on the red dashed lines. But due to manufacturing tolerances, PES data positions can vary. Using the notation $\aleph(\mu, \lambda)$ as detailed above, we model the PES corrupted by timing jitter $\tilde{e}^m$ as

$$\tilde{e}^m = e(t), \quad \text{for} \quad t = (m + kN) \cdot \Delta\tau$$

where the PES sampling interval $\Delta\tau \sim \aleph((v)/(60)N, \delta)$ and v is the speed of a disk.

Detailed simulation results of the timing jitter effect will be presented in Section IV.

C. HDD Case Study

Our goal is to predict PES quality and servo pattern performance at higher track densities for future product planning. PES simulation for the desired track density of 400 kTPI will be conducted as a performance evaluation example. Prediction of PES quality and servo pattern performance of HDDs for high recoding densities is difficult to achieve due to the difficulty of defining accurate models for plants and disturbances. These models are critical for achieving realistic data for future products.

A technical committee of IEE Japan released a benchmark for HDDs in 2005 [17]. In a session of a technical meeting of IEE Japan, the HDD benchmark was presented for track-following control of the plant model (a track density of 100 kTPI) whose frequency response is shown in Fig. 6(a). In the benchmark, torque disturbance, flutter disturbance, repeatable runout (RRO), and sensor noise are considered. The spectrums of these disturbances are shown in Fig. 6(b).

The modified plant, controller and disturbance models for 400 kTPI based on this Japanese benchmark are defined and used to evaluate the closed-loop servo track following performance with different servo patterns. Interpolation of the Japanese benchmark model (100 kTPI) to obtain the physical properties of the HDD (400 kTPI) used in the simulations is defined in Table I. In our interpolation of HDD parameters, the track density and

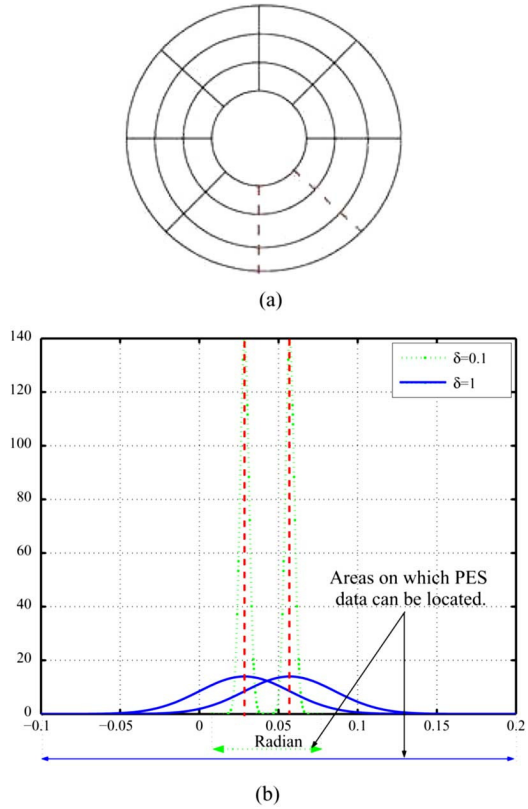

Fig. 5. (a) Hard disk servo sectors. (b) Probability distributions of PES data positions (servo sector locations) at two successive servo sectors indicated in (a). The green dotted lines indicate the probability distribution when the dispersion parameter $\delta = 0.1$ while the blue solid lines indicate the probability distribution when $\delta = 1$. If there is no dispersion in servo sector locations, the PES data positions will be exactly located on the red dashed lines. But due to manufacturing tolerances, PES data positions can vary by following these probability distributions.

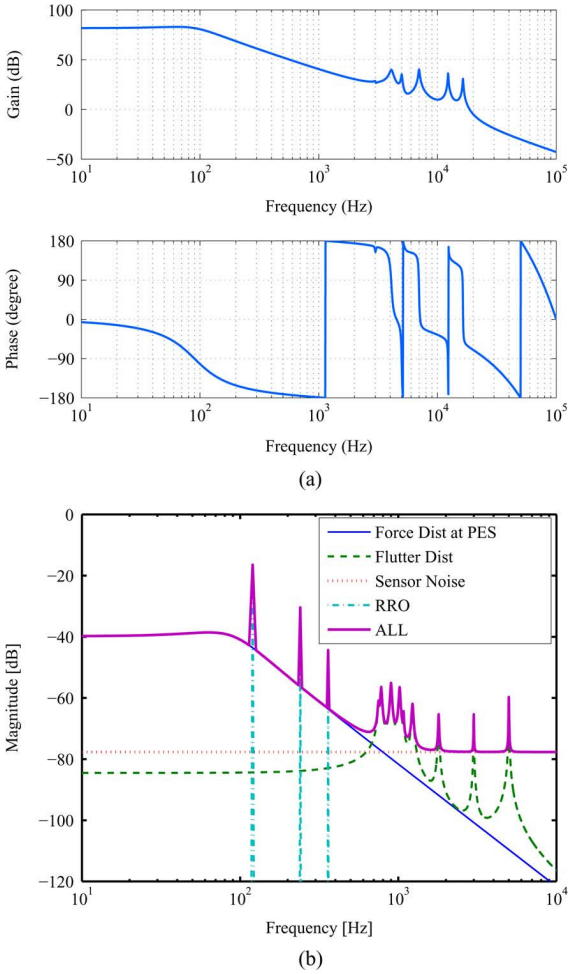

Fig. 6. (a) Japanese benchmark plant model in the frequency domain. (b) Japanese benchmark disturbance data in the frequency domain. The thin blue solid line is force disturbance, the green dashed line is flutter disturbance, the red dotted line is sensor noise, the light blue dashed-dotted line is repeatable run-out (RRO) and the thick purple solid line is total disturbance. (a) Japanese benchmark plant (100 kTPI). (b) Japanese benchmark disturbances (100 kTPI).

spindle speed increase, and the track width decreases. Based on these changes, dynamics of the plant, disturbances and controller were modified.

The block diagram of the closed-loop track following with main components (a plant, a controller, disturbances and readback signal demodulation) is shown in Fig. 7. In the closed-loop track following, disturbance is classified into two categories, the input disturbance $d_i(t)$ and the output disturbance $d_o(t)$. The feedforward signal f^m can be used to cancel the RRO disturbance. After the off-track position $y_p(t)$ is generated, the readback signal $R(k)$ is generated by using the bit pattern signal $b(k)$ and the transition response $h(k, w)$ via the models presented in Section III, and then demodulated to generate PES $\tilde{e}^m$ via the demodulation methods presented in Section II. The track following controller rejects the effect of disturbance and achieves a minimum PES signal.

An overview of simulation results and discussions using this closed-loop track following will be presented in the next section.

IV. Overview of Simulation Results

A. Simulation Results

Simulation has been carried out for our HDD case study with a track density of 400 kTPI to evaluate PES quality and servo

TABLE I
HDD Parameters at 400 kTPI

Parameters	Values	Units
Track density	400	[kTPI]
Track width	63.5	[nm]
Spindle speed	15,000	[rpm]

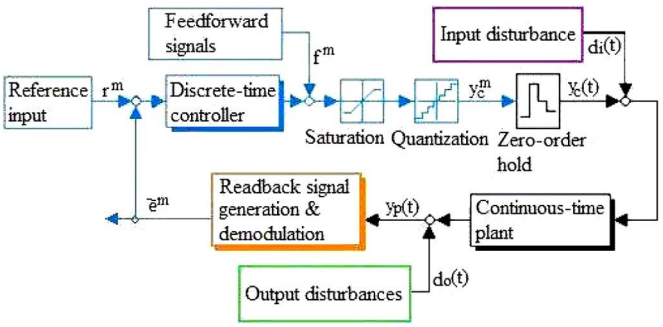

Fig. 7. Block diagram of the closed-loop servo track following with main components (a plant, a controller, disturbances, and readback signal demodulation). The readback signal $R(k)$ is generated by using the bit pattern signal $b(k)$ and the transition response $h(k, w)$, and then demodulated to generate PES $\bar{e}^m$.

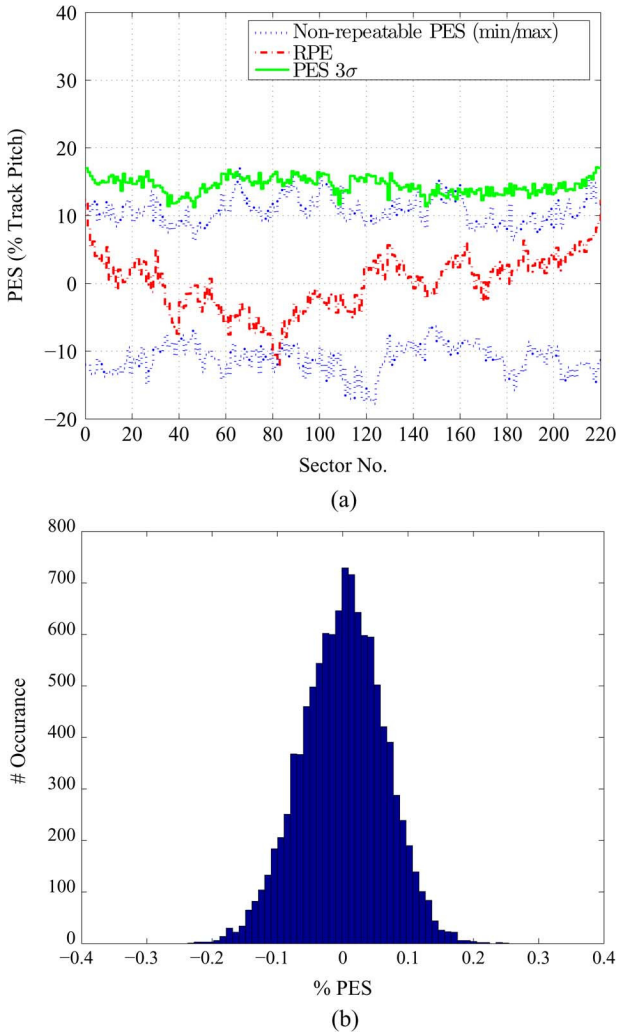

Fig. 8. (a) PES at a track density of 400 kTPI without considering the effect of the quality factors discussed in Section II. The green solid line is the 3σ value of the PES, the red dashed line is repeatable position error, and the blue dotted lines are nonrepeatable position errors (min/max). (b) Histogram of PES at a track density of 400 kTPI. (a) PES (400 kTPI). (b) Histogram (400 kTPI).

pattern performance. The PES and its histogram, without considering any effect of the quality factors discussed in Sections II and III, are shown in Fig. 8. In Fig. 8, a distinction is made between the effects of repeatable and non-repeatable position errors on the PES. From the closed-loop servo track following simulation result, the performance of the HDD case study can be estimated. The 3σ value of the PES is a good indication of servo performance. Running the simulation for multiple revolutions allows the evaluation of the PES 3σ value, including the non-repeatable error. It can be seen in Fig. 8 that the 3σ value of the PES is obtained at around 15% of a track pitch without considering the effect of quality factors. However, the obtained simulation result, without considering the effect of quality factors, is far from being realistic data. In order to provide more realistic simulation results for better performance evaluation, the quality factors must be included.

B. Quality Assessment for PES

In this section, the effects of readback signal quality and timing jitter on PES are investigated. As mentioned in

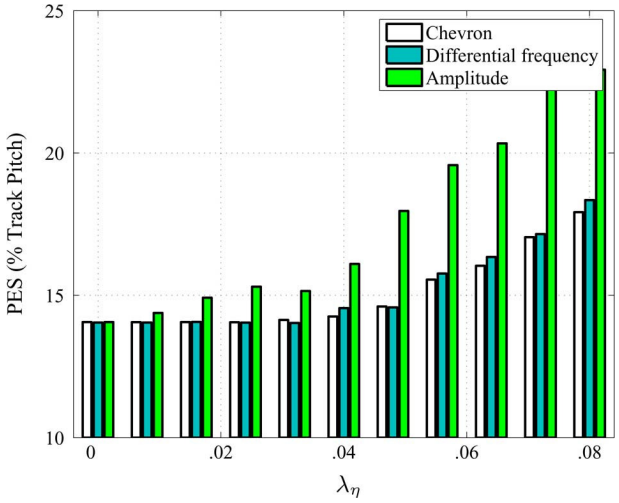

Fig. 9. Amplitude fluctuation noise effect on PES modeled in (1), where λ_η is the variance of amplitude fluctuation noise distribution.

Section II, amplitude fluctuation noise, transition jitter and readback signal sampling are the main quality factors to be considered in readback quality evaluation. The readback signal corrupted by media noise $\tilde{e}^m$ presents amplitude fluctuations. Amplitude fluctuation noise was modeled by white noise on the bit pattern signal $b(k)$ with the variance parameter λ_η and given in (1). The sensitivity of each servo pattern to amplitude fluctuation noise is shown in Fig. 9. In the amplitude servo pattern, amplitude fluctuation noise causes the degradation of PES. However, in time-based servo patterns (chevron and differential frequency servo pattern), amplitude fluctuations due to amplitude fluctuation noise do not greatly affect PES quality, regardless of servo pattern, because the time difference between pulses in the readback signal $R(k)$ is not greatly affected by amplitude fluctuation, as shown in Fig. 9.

On the other hand, transition jitter greatly affects PES quality due to the usage of time-based servo patterns and readback signal demodulation methods because transition jitter causes phase shift of readback signals. Transition jitter was modeled by white noise time shift in the transition response $h(k, w)$ with the variance parameter λ_γ and given in (2). The sensitivity of each servo pattern to transition jitter is shown in Fig. 10. Both the chevron and differential frequency servo patterns are very sensitive to transition jitter, as shown in Fig. 10. The differential frequency servo pattern is slightly less sensitive to transition noise than the chevron pattern because each magnetic bar in the chevron servo pattern is placed closer to neighboring bars than each magnetic bar in the differential frequency. However, even though the sensitivity of each servo pattern to the transition jitters is high, the variation of transition jitter distribution will be dramatically reduced in BPM, close to zero. Thus, transition jitter effect on PES will stay low. Reducing transition jitter effect on PES is another significant advantage of using BPM.

Also, readback signal sampling greatly affects the signal quality in time-based servo patterns. We investigated the readback signal sampling effect on PES by changing the number of samples N_p used to sample the bit pattern signal $b(k)$ given in (3). The sensitivity of each servo pattern to readback signal

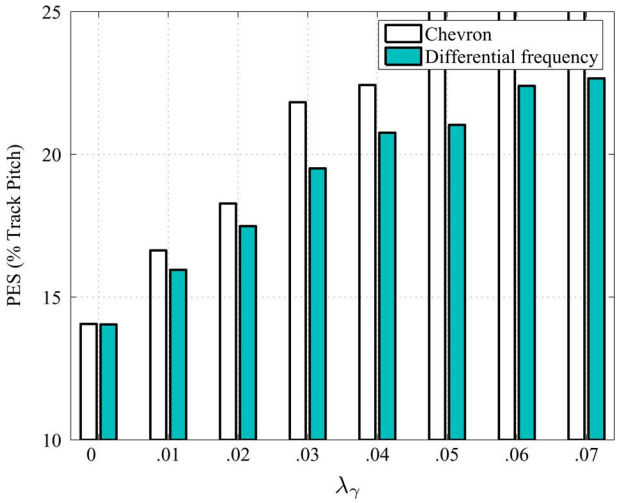

Fig. 10. Transition jitter effect on PES modeled in (2), where λ_γ is the variance of transition jitter distribution. The unshaded and shaded bars indicate the PES generated from the chevron and differential frequency servo patterns, respectively.

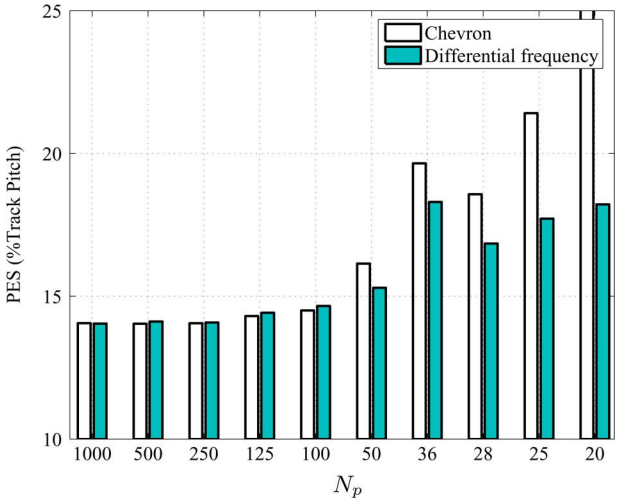

Fig. 11. Readback signal sampling effect on PES. N_p is the number of samples used to sample the bit pattern signal $b(k)$ modeled in (3). The unshaded and shaded bars indicate the PES generated from the chevron and differential frequency servo patterns, respectively.

sampling is shown in Fig. 11. The differential frequency pattern is less sensitive than the chevron pattern to readback signal sampling, as shown in Fig. 11, also because each magnetic bar in the chevron servo pattern is placed closer to neighboring bars than each magnetic bar in the differential frequency servo pattern.

Fig. 12 shows the timing jitter effect on PES. PES quality degrades as the dispersion parameter increases (as the variation in PES data positions increases), regardless of servo patterns used because the variation in the PES sampling interval $\Delta\tau$ does not depend on servo patterns.

V. Conclusion

The objective of this paper was to evaluate the quality of PES generated by several different servo patterns from a closed-loop (servo) point of view, thereby advancing the integration of

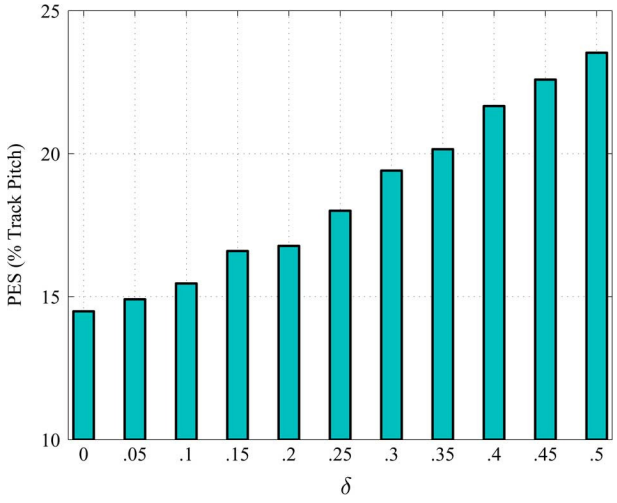

Fig. 12. Timing jitter effect on PES. δ is the dispersion parameter modeled in (4). The PES quality degrades as the dispersion parameter δ increases regardless of the servo patterns used.

BPM in HDDs by aiding in the selection of a servo pattern that provides sufficient PES quality. PES quality was evaluated by investigating important quality factors: amplitude fluctuation noise, transition jitter, readback signal sampling, and timing jitter. Three servo patterns (the amplitude pattern, chevron pattern, and differential frequency pattern) were considered as case studies. Evaluation of PES quality and track following performance for each servo pattern at a track density of 400 kTPI was conducted by using an advanced PES simulation tool developed in our lab to provide realistic simulation of HDD track following. The timing-jitter resulting from misalignment of the servo sector locations due to manufacturing tolerances was found to degrade PES quality regardless of servo patterns used. Due to PES nonlinearity in the amplitude servo pattern, time-based servo patterns are considered as alternatives. For time-based servo patterns, readback signal sampling and transition jitter were found to greatly affect PES quality. On the other hand, amplitude fluctuation noise was not found to greatly affect PES quality. Therefore, we conclude that the differential frequency servo pattern is superior to other patterns, since it is less sensitive to transition jitter and readback signal sampling. Also, when printing servo patterns on a disk repeatedly, the differential frequency pattern has an advantage in alignment. Future work on investigating the effect of position and shape variation of patterned bits is required for better servo pattern performance evaluation and guiding fabrication process.

Acknowledgment

This work was supported by a grant from the EHDR Information Storage Industry Consortium (INSIC).

References

[1] A. Mamun, G. Guo, and C. Bi, *Hard Disk Drive: Mechatronics and Control*. Boca Raton, FL: CRC, 2007.

[2] R. Sbiaa and S. Piramanayagam, "Patterned media towards nano-bit magnetic recording: Fabrication and challenges," *Recent Patents Nanotechnol.*, vol. 1, pp. 29–40, 2007.

[3] A. Barany and H. Bertram, "Transition position and amplitude fluctuation noise model for longitudinal thin film media," *IEEE Trans. Magn.*, vol. 23, no. 5, pp. 2374–2376, Sep. 1987.

[4] Y. T. C. Tsang, "Disk-noise induced peak jitters in high density recording," *IEEE Trans. Magn.*, vol. 29, no. 6, pp. 3975–3977, Nov. 1993.
[5] A. Sacks and W. Messner, "MR head effects on PES generation: Simulation and experiment," *IEEE Trans. Magn.*, vol. 32, no. 3, pp. 1773–1778, May 1996.
[6] K. Akagi, K. Yasuna, and K. Shishida, "Optimizing servo-signal design for a hard-disk drives," *Microsyst. Technol.*, vol. 11, pp. 784–789, 2005.
[7] J. Zhu, X. Lin, L. Guan, and W. Messner, "Recording, noise, and servo characteristics of patterned thin film media," *IEEE Trans. Magn.*, vol. 36, no. 1, pp. 23–29, Jan. 2000.
[8] M. Moneck, J. Zhu, Y. Tang, K. Moon, H. Lee, S. Zhang, X. Che, and N. Takahashi, "Lithographically patterned servo position error signal patterns in perpendicular disks," *J. Appl. Phys.*, vol. 103, pp. 07C511–07C511-3, 2008.
[9] H. Richter, A. Dobin, O. Heinonen, K. Gao, R. V. D. Veerdonk, R. Lynch, J. Xue, D. Weller, P. Asselin, M. Erden, and R. Brockie, "Recording on bit-patterned media at densities of 1 Tb/in^2 and beyond," *IEEE Trans. Magn.*, vol. 42, no. 10, pp. 2255–2260, Oct. 2006.
[10] O. Heinonen and K. Gao, "Extensions of perpendicular recording," *J. Magn. Magn. Mater.*, vol. 320, pp. 2885–2888, 2008.
[11] A. Kikitsu, Y. Kamata, M. Sakurai, and K. Naito, "Recent progress of patterned media," *IEEE Trans. Magn.*, vol. 43, no. 9, pp. 3685–3688, Sep. 2007.
[12] E. Hughes and W. Messner, "New servo pattern for hard disk storage using pattern media," *J. Appl. Phys.*, vol. 93, pp. 7002–7004, 2003.
[13] X. Lin, J. Zhu, and W. Messner, "Investigation of advanced position error signal patterns in patterned media," *J. Appl. Phys.*, vol. 87, pp. 5117–5119, 2000.
[14] E. Hughes and W. Messner, "Characterization of three servo patterns for position error signal generation in hard drives," in *Proc. American Control Conf.*, Denver, CO, 2003, pp. 4317–4321.
[15] W. Messner, J. Zhu, and X. Lin, "Frequency Modulation Pattern for Disk Drive Assemblies," U. S. Patent 6,754,016B2, 2004.
[16] B. Bane Vasic and E. Kurtas, *Coding and Signal Processing for Magnetic Recording Systems*. Boca Raton, FL: CRC, 2005.
[17] *Japan HDD Benchmark Problem*, [Online]. Available: http://mizugaki.iis.u-tokyo.ac.jp/nss/